Nano Energy 106 (2023) 108062

Contents lists available at ScienceDirect

Nano Energy

journal homepage: www.elsevier.com/locate/nanoen

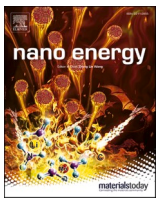

Revivification of nickel oxide-perovskite interfaces via nickel nitrate to boost performance in perovskite solar cells

Dilpreet Singh Mann, Sung-Nam Kwon *, Pramila Patil, Seok-In Na *

Department of Flexible and Printable Electronics and LANL-JBNU Engineering Institute-Korea, Jeonbuk National University, 567, Baekje-daero, Deokjin-gu, Jeonju-si 54896, Republic of Korea

ARTICLE INFO

Keywords:
Perovskite solar cells
Nickel oxide
Nickel nitride
Surface defects
Hydroxyl groups
Charge carrier dynamic

ABSTRACT

Nickel oxide (NiO_x) is a prospective hole transporting layer (HTL) material for inverted (p-i-n) perovskite solar cells (PSCs); however, inevitable surface defects on the NiO_x surface interfere with the realization of high-performance PSCs. Herein, nickel nitrate is used to eliminate defect sites and hydroxyl groups on the NiO_x surface. For the first time, it is found that a uniform and ultra-thin nickel nitride (Ni_xN) layer can be formed on the NiO_x surface through the spin coating of the nickel nitrate solution at low temperatures. Promisingly, this new approach allows to overcome interface losses originating from defect sites and hydroxyl groups on the NiO_x surface and to achieve high efficiency and long-term operational stability in PSCs. Furthermore, Ni_xN serves better energy level alignment between NiO_x HTL and perovskite layer, resulting in improved charge extraction and transportation and reduced charge recombination. The Ni_xN-modified NiO_x-based PSC demonstrates an outstanding efficiency of 20.45% and it shows long-term operational stability about 82% of the initial efficiency after 1000 h under ambient air conditions. Thus, this simple approach using nickel nitrate can be a promising and universal strategy to revive nickel oxide-perovskite interfaces and boost the performance and operational stability of PSCs.

Introduction

Perovskite solar cells (PSC) are growing as a competitor to commercial solar technology through the combination of high efficiency and low-cost solution processes. PSCs have recently reached power conversion efficiency (PCE) of up to 25.7% at a surprisingly high speeds, eventually comparable to commercial silicon solar cells [1]. Nickel oxide (NiO_x) thin films have used a hole transport layer (HTL) for the p-i-n junction PSC, as an alternative to expensive ultra-thin organic layers that are problematic in stability and scalability [2]. This is because NiO_x has a wide bandgap (E_g, 3.6–4.0 eV) and a deep valence band maximum (VBM, 5.1–5.4 eV), enabling high optical transparency and effective charge extraction [3,4]. In addition, NiO_x HTLs can be deposited via techniques widely used in the industry, such as spin coating, spray coating, atomic layer deposition (ALD), and sputtering [5–9]. However, NiO_x HTL-based PSCs are generally difficult to achieve high efficiency due to interfacial loss [10–12]. Inevitable surface defects and charged chemical species (OH^-, H^+, and ions) of NiO_x interfaces obstruct to achieve high PCE and long-term operational stability [13]; surface defects increase charge recombination and reduce open-circuit voltage (V_{OC}), fill factor (FF), and short-circuit current density (J_{SC}) [14–17]; charged chemical species lead to decomposition of perovskite and degrade the stability of the PSC [16,18]. Thus, developing advanced technology to engineer the interface of NiO_x HTL is a promising strategy to improve the performance of PSCs.

Numerous studies have been conducted to improve the interface characteristics of NiO_x HTL. Doping and the use of composites are the most common and widely used strategies, as they lead to enhanced overall performance of NiO_x-based PSCs [19–21]. Yao et al. reported that Cu-doped NiO_x enhances the charge collection at the NiO_x/perovskite interface and reduces recombination loss, achieving efficiency up to 18.1% [22]. We demonstrated that the NiO_x nanoparticle (NPs) and boron nitride (BN) composite HTL can improve efficiency by enhancing energy level alignment and interface contact between the HTL and the perovskite layer [23]. However, interface losses originating from defect sites and hydroxyl groups on the NiO_x surface remain a challenge to address in order to achieve high PCE and long-term operational stability [23,24].

Surface modification is a direct approach to engineer the interface of NiO_x HTL and improve the efficiency and stability of PSCs. Wang et al.

* Corresponding authors.
E-mail addresses: dasom2u@jbnu.ac.kr (S.-N. Kwon), nsi@jbnu.ac.kr (S.-I. Na).

https://doi.org/10.1016/j.nanoen.2022.108062
Received 20 June 2022; Received in revised form 23 November 2022; Accepted 28 November 2022
Available online 5 December 2022

used the benzoic acid, self-assemble molecule (SAM), as a surface modifier in the NiO_x/perovskite interface, resulting in a rise in V_{OC} [25]. Singh et al. investigated interface reinforcement using SAM. They showed that para-substituted phenylphosphonic acids can provide better energy band alignment and charge transportation, resulting in PCE up to 18% [26]. Cheng et al. reported that the pyridine-terminated conjugated small organic molecules can reduce the defect density and charge recombination [27]. We also demonstrated that the 3-(Triethoxysilyl)propylamine SAM introduced between NiO_x and perovskite film as the interface modifier can reduce the defect sites and prevent degradation by direct contact of hydroxyl groups of NiO_x surface and the perovskite layer [13]. However, the surface modifiers based on these organic molecules are not suitable for ensuring long-term stability of PSCs due to their self-decomposition in a continuous light irradiation environment, especially for p-i-n PSC in which light transmits HTL [24, 28].

Based on previous studies like this, we modeled a novel approach to overcome interface losses and achieve high PCE and long-term operational stability in PSCs. Here, for the first time, we report that nickel nitrate deposited by a simple solution process can very effectively eliminate defect sites and hydroxyl groups on the NiO_x surface. Nickel nitrate acted as an interface modifier between NiO_x and perovskite layer, and reacted with defect sites and hydroxyl groups to form a uniform nickel nitride (Ni_xN) ultra-thin layer on the NiO_x surface. Where, metal nitrides, including Ni_xN, possess excellent electrical conductivity compared to corresponding metal oxides, and have higher electrocatalytic activities and stabilities in reduction reactions compared to corresponding pure metals; nitrogen increases the electron density of the surface, which changes the electronic properties of the metal [29–31]. A recent study on PSCs with TiN_x deposited by vacuum process suggests that Ni_xN, a transition metal nitride, could be a promising interface modification layer with excellent electrical and optical properties and chemical stability [32]. Nevertheless, no studies applying Ni_xN to PSCs have been reported, nor have implementation techniques for thin film deposition been reported. In this study, we demonstrated for the first time that the Ni_xN ultra-thin film can be formed on the NiO_x surface through the spin coating of the nickel nitrate solution at low temperatures. XPS analysis proved that nitrogen atoms existed in various chemical states depending on the depth from the surface of the NiO_x NPs thin film, and that Ni_xN ultra-thin film was formed on the surface of NiO_x NPs thin film. In addition, it was observed that when Ni_xN was applied to the surface of NiO_x thin film, Ni^{3+} chemical species on the surface of NiO_x thin film increase, while $Ni^{\geq 3+}$ chemical species decrease. As a result, it was found that a simple nickel nitrate treatment on the NiO_x surface caused the formation of ultra-thin Ni_xN film, effectively reducing defect sites and hydroxyl groups on the surface of the NiO_x thin film. Furthermore, Ni_xN served better energy level alignment between NiO_x HTL and perovskite layer, resulting in improved charge extraction and transportation capability and reduced charge recombination. The Ni_xN-modified NiO_x-based PSC showed an outstanding efficiency of 20.45%. Notably, the high performance obtained for our p-i-n structure devices, among the highest efficiency for inorganic interface modification layer-based PSCs reported to this date, was achieved without additive engineering or post-treatment strategies. Furthermore, this breakthrough approach has increased the operational stability of NiO_x-based PSCs. The Ni_xN-modified NiO_x-based devices achieved steady-state photocurrent density of 20.30 mA cm^{-2} with 19.10% PCE and maintained about 69% of initial efficiency after 120 h continuous light irradiation. In addition, the unencapsulated Ni_xN-modified NiO_x--based PSC maintained about 82% of the initial efficiency after 1000 h under ambient air conditions, whereas the pristine NiO_x-based device maintained only about 60% of the initial efficiency. Further, pristine NiO_x-based PSCs almost deteriorated after 200 h at 85ºC, but the Ni_xN-modified NiO_x-based device maintained more than 40% of its initial PCE in a harsh heat environment. These results demonstrate that this novel approach using nickel nitrate can be a promising and universal strategy to revive nickel oxide-perovskite interfaces and boost the performance and operational stability of PSCs.

Result and Discussion

A number of defects and hydroxyl groups on the nickel surface absorb photons and reduce transmittance of the thin film, which is one of the factors that consequently lowers the efficiency of the photovoltaic device [2]. To confirm this and determine the effectiveness of nickel nitrate (NiN) treatment, we evaluated UV-ozone (UVO) treated NiO_x NPs thin films as a control group and NiO_x NPs thin films treated by NiN as a target group. In addition, the FAI-treated NiO_x NPs thin films reported in a previous study were evaluated as a comparison group [2]. Fig. 1a shows optical images according to the surface condition of the NiO_x NPs thin film. Upon the UVO treatment, it was observed that the NiO_x NPs thin film became physically dark, suggesting the formation of a number of sub-band gap states. The UV–vis absorption spectrum of UVO showed light absorption due to the increase in sub-band gap absorption (Fig. 1b), which is in good agreement with the previous report [2]. Meanwhile, it was observed that physical darkness of the UVO-treated NiOx film was recovered by FAI treatment, indicating a decrease in sub-band gap absorption. However, the FAI-treated NiO_x NPs thin film was slightly orange, which means that the sub-band gap states had not completely recovered. In comparison, encouragingly, the NiN- treated NiO_x NPs thin film exhibited a color relatively similar to that of the pristine NiO_x NPs thin film; the UVO-treated black NiO_x NPs thin film was transparently bleached (Fig. 1a). Further, the overall light absorption decreased with a significant decrease of light absorption in the ultraviolet region (Fig. 1b). It can thus be inferred that NiN reacts with NiO_x like FAI to remarkably bleach the film and reduce the defect density of the NiO_x surface, which is a factor of the sub-band gap. It has been reported that the change in absorption is due to an increase in $Ni^{\geq 3+}$ defect sites, [2] which is consistent with the photoelectron spectroscopy (XPS) results described below.

We utilized high-resolution XPS to estimate changes in chemical composition and nickel oxidation species on the NiO_x surface due to chemical interaction of NiN and NiO_x. Fig. 1c-d show XPS spectra of the representative core level (Ni 2 $p_{3/2}$, O 1 s, and N 1 s) for pristine NiO_x NPs thin films and NiN- treated NiO_x NPs thin films. The fitted Ni $2p_{3/2}$ spectrum showed at least three distinct chemical species, including NiO (green), Ni_2O_3 (purple), and NiOOH (orange) at 853.7, 855.4, and 856.5 eV, respectively (Fig. 1c) [33,34]. Here, NiOOH can take the form of β-NiOOH or γ-NiOOH; this is classified as an $Ni^{\geq 3+}$ defect [2]. The relative chemical composition and relative ratio of nickel oxidation species for the fitted Ni $2p_{3/2}$ and O 1 s core level spectra (Fig. 1c-d) are reported in Table S1. High BE satellite peaks with binding energies above 860 eV were ignored because they were associated with unblocked Ni components and were generally not considered in the analysis of Ni oxidation states [35]. As deposition of NiN onto the pristine NiO_x NPs thin film, the relative composition of the chemical species corresponding to NiO (Ni^{2+}) and NiOOH ($Ni^{\geq 3+}$) decreased, and the content of Ni_2O_3 (Ni^{3+}) increased. More specifically, the ratio of nickel oxide species of Ni_2O_3 to NiO increased from 0.59 (pristine) to 0.72 (with NiN), while that of NiOOH decreased from 0.56 (pristine) to 0.54 (with NiN). Furthermore, changes in chemical composition and relative ratio of nickel oxidation species for the Ni $2p_{3/2}$ of the NiO_x NPs thin film according to NiN treatment were generally consistent with values determined in the corresponding O1s spectrum analysis (Fig. 1d and Table S1). As a result, it can be seen that, after NiN treatment, Ni^{3+} chemical species increased while $Ni^{\geq 3+}$ chemical species decreased, which suggests that defect sites and hydroxyl groups on the surface of the NiO_x NPs thin film decreased and charge transfer characteristics improved at the same time [36]. Further, it can be inferred that electrochemical reduction of $Ni^{\geq 3+}$ defects was induced by oxidation of nickel nitrate.

Consistent with this, the significant increase in the N 1 s signal after

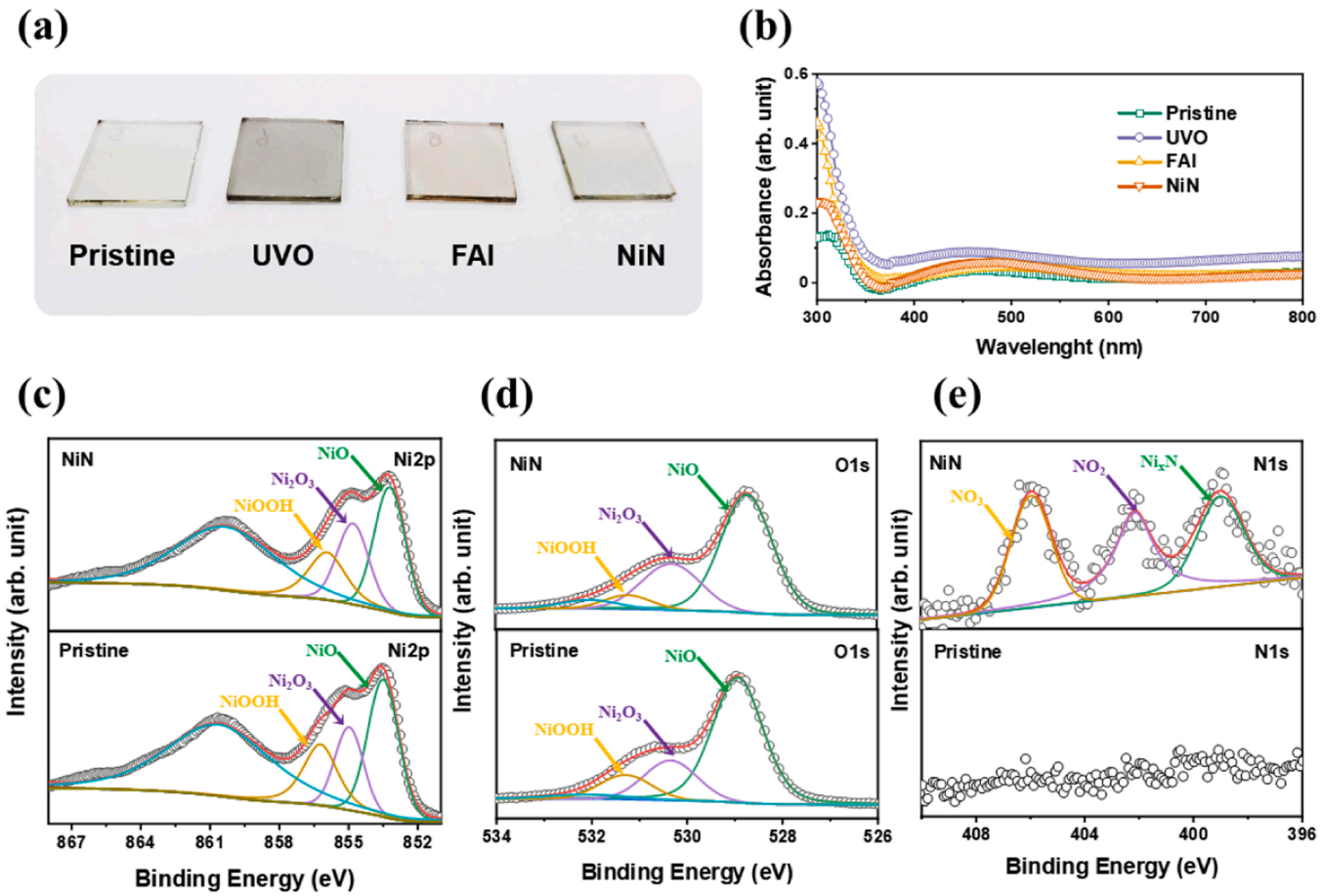

Fig. 1. (a) Photograph and (b) UV–visible spectra of as-deposited pristine NiO_x NPs thin films and NiO_x NPs thin films treated with UVO, FAI and NiN. (c) High-resolution X-ray photoelectron spectroscopy (XPS) spectra of Ni $2p_{3/2}$, (d) O 1s, and (e) N 1s of pristine and NiN-treated NiO_x NPs thin films.

NiN treatment, as shown in Fig. 1e, indicates the presence of nitrogen adducts produced through chemical interactions between nickel nitrate and chemical species (defect sites and hydroxyl groups) present on the surface of NiO_x NPs thin films. Similar to previous studies [37–39], the N 1 s spectrum of the NiN- treated NiO_x NPs thin film showed the presence of NO_3^-, NO_2^-, and Ni_xN peaks at ~405.1, – 402.5, and 398.5 eV, respectively (Fig. 1e), which indicates that nitrogen atoms existed on the surface of the NiO_x NPs thin film in various chemical states. Angle resolved X-ray photoelectron spectroscopy (ARXPS) provided details of the chemical interaction of NiN deposited on the surface of NiO_x NPs thin films and the formation of nitrogen-derived chemical species (Fig. S1). Detection depth of sample was controlled by changing the sample tilt angle ($\alpha = 0°$, 15°, 30°, 45°, and 60°) with reference to the analyzer. As shown in Figure S1, when the sample tilt angles are 45° and 60°, only the Ni_xN peak is observed, confirming that only Ni_xN exists on the surface of the NiO_x layer. In addition, from the relationship between sample tilt angle and depth profile, it can be inferred that Ni_xN forms a thin film with a thickness of 6 nm or less. In contrast, low intensity NO_3^- and NO_2^- peaks were observed when the sample tilt angle is lower than 45°, which indicates that they formed below a depth of 6 nm. From this, it can be suggested that nitrogen atoms originated from nickel nitrate diffuse to a depth of 6 nm or more from the surface of the NiO layer and form a small amount of nitrogen oxide species such as NO_3^- and NO_2^-. Here, since nitrogen has a more negative valence state (N^{3-}) than oxygen (O^{2-}), N^{3-} that has penetrated into the NiO_x crystal lattice occupies an O^{2-} site, and as a result, the number of Ni^{2+} vacancies increases, which in turn increases the Ni^{3+} content [40]. The increase in the Ni^{3+} content of the Ni_xN-modified NiO_x thin film means that the conductivity of the thin film can be increased at a depth of more than 6 nm, thereby improving charge transfer [41]. On the other hand, interestingly, the main properties of the interface are affected by the physicochemical state of the thin film surface, and it was designated as a representative effect by focusing on the Ni_xN generated on the surface rather than the small nitrogen oxide species inside. These observations prove that nitrogen atoms exist in various chemical states depending on the depth from the surface of the NiO_x NPs thin film, and that the Ni_xN ultra-thin film is formed on the surface of the NiO_x NPs thin film. It may also be deduced that the nickel nitride layer can passivate the NiO_x surface, eliminating hydroxyl groups and reducing the surface defect ($Ni^{\geq 3+}$) sites. Furthermore, the energy dispersion X-ray spectroscopy image supported that nitrogen atoms were uniformly distributed on the NiO_x surface (Fig. S2), and as a result, suggested that nickel nitride (Ni_xN) was uniformly deposited on the NiO_x surface. From here on, NiO_x NP_S thin films with Ni_xN formed on the surface through NiN treatment are called Ni_xN-modified NiO_x thin films. To determine changes in physical and electrical properties of the NiO_x NPs thin film according to NiN deposition, we performed atomic force microscopy (AFM), scanning Kelvin probe microscopy (SKPM), and ultraviolet-visible spectroscopy (UPS) analyses. There were no significant changes in the physical surface properties between the pristine NiO_x NPs thin film and the Ni_xN-modified NiO_x thin film. The root-mean-square roughness (rms) values of the pristine and Ni_xN-modified NiO_x NPs thin films were 3.47 and 2.56 nm, respectively (Fig. 2a), indicating that the Ni_xN-modified NiO_x NPs thin film had a slightly smoother surface than those of the pristine NiO_x NPs thin films. The smoother surface of the modified NiO_x layer can result in reduced recombination and increased hole extraction [23,42]. Meanwhile, the electrical characteristics of the surface showed a significant change with NiN deposition (Fig. 2b). The Ni_xN-modified NiO_x NPs thin

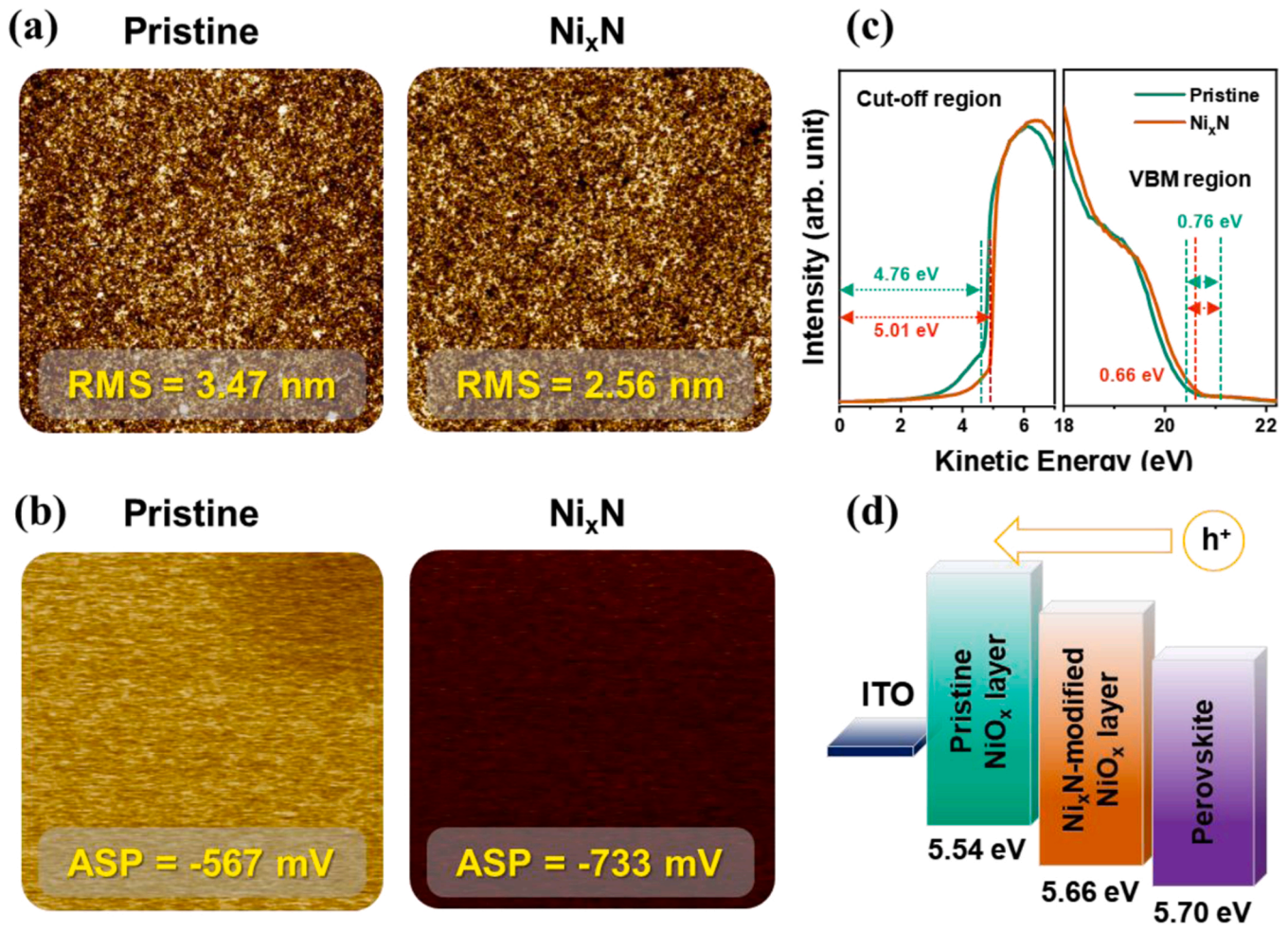

Fig. 2. (a) Atomic force microscopy (AFM) and (b) Scanning Kelvin probe microscopy (SKPM) images of pristine and Ni_xN-modified NiO_x NPs thin films (ASP is average surface potential). (c) Ultraviolet photoelectron spectroscopy spectra of pristine and Ni_xN-modified NiO_x NPs thin films. (d) Schematic energy level diagram of pristine and Ni_xN-modified NiO_x NPs thin films with perovskite.

film showed a lower surface potential value (−733 mV) than that of the pristine NiO_x NPs thin film (−567 mV), which implies a deeper work function (WF) of Ni_xN-modified NiO_x than that of pristine NiO_x [43,44]. This result was well consistent with the UPS analysis (Fig. 2c). The cut-off edge of Ni_xN-modified NiOx shifted to higher kinetic energy, resulting in a higher WF (5.01 eV) than that of pristine NiO_x (4.76 eV). In addition, the corresponding balance band maximum (VBM) of the Ni_xN-modified NiO_x NPs thin film was shifted downward by about 0.12–5.66 eV. These results suggest that the energy level of Ni_xN-modified NiO_x is well suited to perovskite layers, as shown in the band diagram in Fig. 2d. Meanwhile, the thin film thickness of Ni_xN is less than 6 nm, which wouldn't be sufficient to form a depletion region. Therefore, it is speculated that the Ni_xN-modified NiO_x layer tunes WF and acts as a charge tunneling passivation layer. Ni_xN-modified NiO_x layer at perovskite/NiOx interface, which could selectively tunnel holes meanwhile blocking electrons to form a well-aligned energy level and suppressing carrier recombination [45,46]. From these observations, it can be inferred that Ni_xN-modified NiO_x can provide the pathway to improve the charge extraction from perovskite to NiO_x layer, which leads to interface resistance reduction and increased built-in potential, suggesting that it may lead to improvements in V_{OC}, J_{SC}, and FF, and consequently may contribute to the efficiency improvement of PSCs [47].

Following the determination of chemical and electrical changes in the NiO_x surface by NiN treatment, pristine NiO_x and Ni_xN-modified NiO-based PSCs were evaluated to ensure that the inference derived from the above results correspond to the device performance. We fabricated a series of PSCs with p-i-n architecture (glass/ITO/NiO_x/triple-cation perovskite/Phenyl-C61-butyric acid methyl ester; $PC_{61}BM$/ZnO NPs/Ag), as shown in the image inserted in Fig. 3a, and tested NiO_x NPs thin films with various concentrations of nickel nitrate (5, 10, 15, and 20 mmol). Deposition of NiN, with 10 mmol as the optimum concentration, resulted in dramatic improvements in V_{OC} from 1.06 to 1.12 V and overall power conversion efficiency (PCE) from 17.2% to 18.92% (Fig. S3). To better study the performance improvement with NiN deposition, a more detailed statistical analysis of over 15 devices was carried out under optimal conditions. The current density-voltage (J-V) curve of the best devices, measured under AM 1.5 G illumination at 100 mW cm^{-2}, are illustrated in Fig. 3a; the histograms of the photovoltaic parameters of the devices with pristine NiO_x and Ni_xN-modified NiO_x are presented in Fig. 3b and Fig. S4. Additionally, the corresponding photovoltaic parameters of the best device are listed in Table S2. For all photovoltaic parameters, devices with Ni_xN-modified NiO_x performed significantly better than devices with pristine NiO_x. This performance improvement was more pronounced when comparing the best-performing device with and without NiN. The pristine NiO_x-based device showed a PCE of only 18.32%, with V_{OC} of 0.97 V, J_{SC} of 23.35 mA cm^{-2}, and FF of 78.01%. While, remarkably, the Ni_xN-modified NiO_x-based device showed significantly improved V_{OC} of 1.06 V, J_{SC} of 24.34 mA cm^{-2}, and FF of 79.18%, resulting in an enhanced PCE of 20.45%, up 10% from the comparative group. These results were well supported by the external quantum efficiency (EQE)

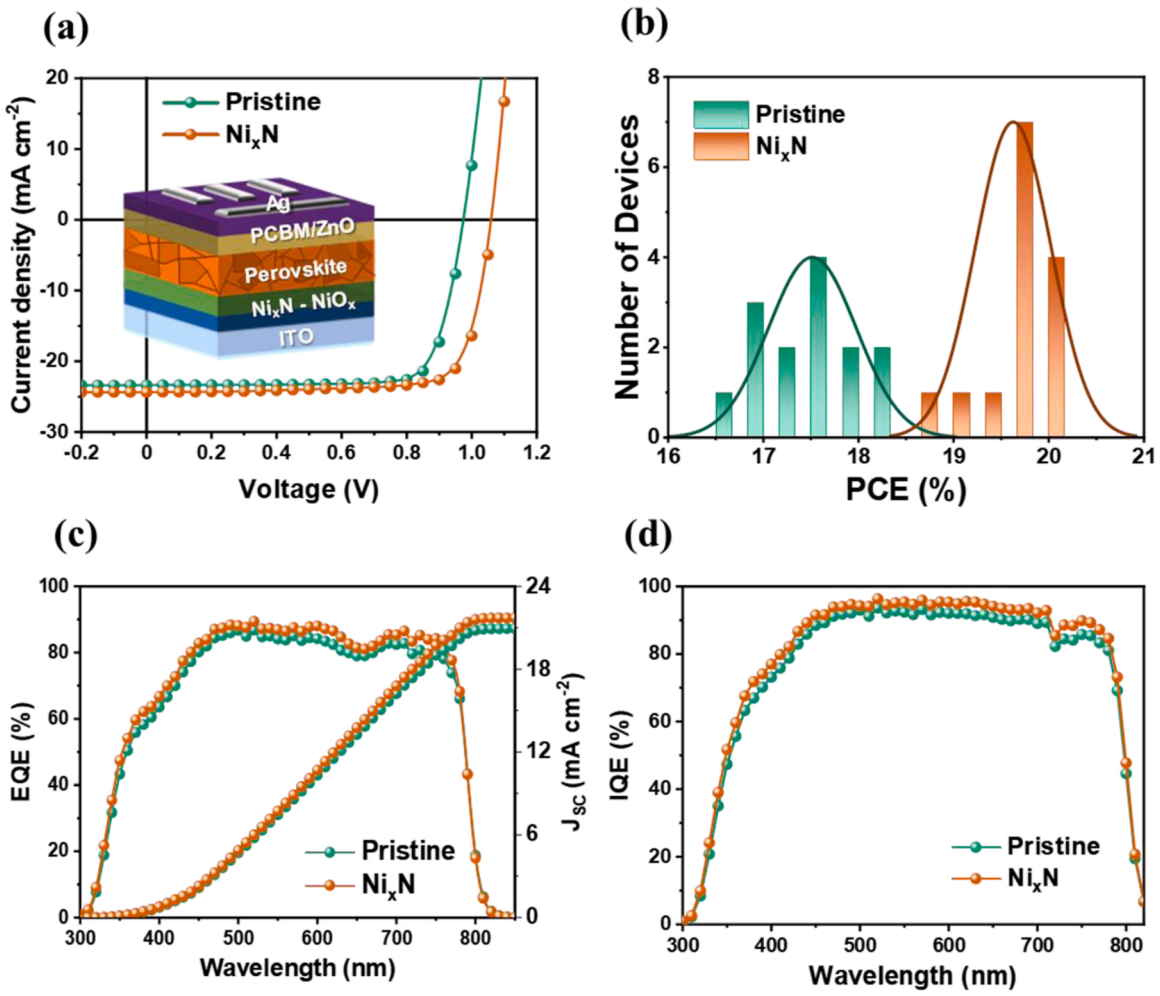

Fig. 3. (a) Current-voltage (J-V) curves of the pristine and Ni_xN-modified NiO_x-based devices under optimal conditions (insert figure is the schematic device architecture of p-i-n PSCs). (b) Corresponding statistical histogram of PCEs. (c) External and (d) internal quantum efficiency curves of corresponding pristine and Ni_xN-modified NiO_x-based devices.

and similar absorbance spectra (Fig. S5); the EQE of the Ni_xN-modified NiO_x-based device showed a better charge harvesting ability than that of the pristine NiO_x-based device as shown in Fig. 3c. To find factors that improve the charge harvesting ability of the Ni_xN-modified NiO_x-based device, the internal quantum efficiency (IQE) was measured (Fig. 3d). The IQE spectrum of the device with Ni_xN also presented improved efficiency in a wide wavelength range similar to that of the EQE spectrum. Crucially, the efficiency improvement ratios of EQE and IQE were similar at about 1.05, indicating that efficiency enhancement resulting from the deposition of NiN is mainly due to improvements in charge extraction and transport capability [13,48]. These results also prove that the improved performance of Ni_xN-modified NiO_x-based devices can be attributed to the reduced surface defect sites and the well-matched energy level in the Ni_xN-modified NiO_x/Perovskite interface [13,49].

To investigate the photo-induced charge extraction and transport dynamics, transient photocurrent (TPC) and transient photovoltage (TPV) measurements were performed (Fig. 4a-b). TPC allows the measurement of time-dependent charge extraction characteristics of photo-induced charge carriers in solar cells [50], while TPV allows direct monitoring of the lifetime of photo-induced charge carriers by measuring changes in photovoltage of the solar cell [51]. The long TPC and TPV decay times indicate, respectively the slow charge extraction and transport properties and the lower charge-carrier recombination, respectively [49,52,53]. From this point of view, the Ni_xN-modified NiO_x-based device (decay time = 1.15 μs) has been confirmed to have faster charge extraction and transport properties compared to the NiO_x-based device (decay time = 1.61 μs). Furthermore, the Ni_xN-modified NiO_x-based device had a longer TPV decay time (0.21 ms) than that of the NiO_x-based device (0.14 ms), suggesting that charge-carrier recombination had been reduced. These results are consistent with PL measurements indicating enhanced charge extraction and transfer (Fig. S6) [54–56]. Photo-CELIV, which measures photogeneration and carrier extraction by linearly increasing the voltage under illumination, can even better illustrate the charge carrier dynamics of the device under operation conditions (Fig. 4**c**). The inset images in Fig. 4c show the current density curve at maximum peak (Δj), in which the area of the curve corresponding to Δj is proportional to the extractable charge (Q_{ext}), and the large areas indicate low charge recombination [57]. From this, it can be estimated that Q_{ext} of the device with Ni_xN is greater than that of the device with pristine NiO_x. Further, it was found that the charge carrier mobility of the device with Ni_xN, which calculated by the equation with the Δj and t_{max} that is the time when the value of the current density is maximum [58–60]. was faster than that of the device with pristine NiO_x. Charge-carrier mobility values of the Ni_xN-modified NiO_x-based device and pristine NiO_x-based device were 3.05×10^{-4} and 1.24×10^{-4} cm^2 V^{-1} s^{-1}, respectively. These results reveal that the Ni_xN-modified NiO_x-based device has better charge extraction and lower charge recombination [57,61]. Moreover, it can be proved that Ni_xN facilitates charge extraction and transport as well as reducing charge-carrier recombination, thereby improving V_{OC}, J_{SC}, and FF.

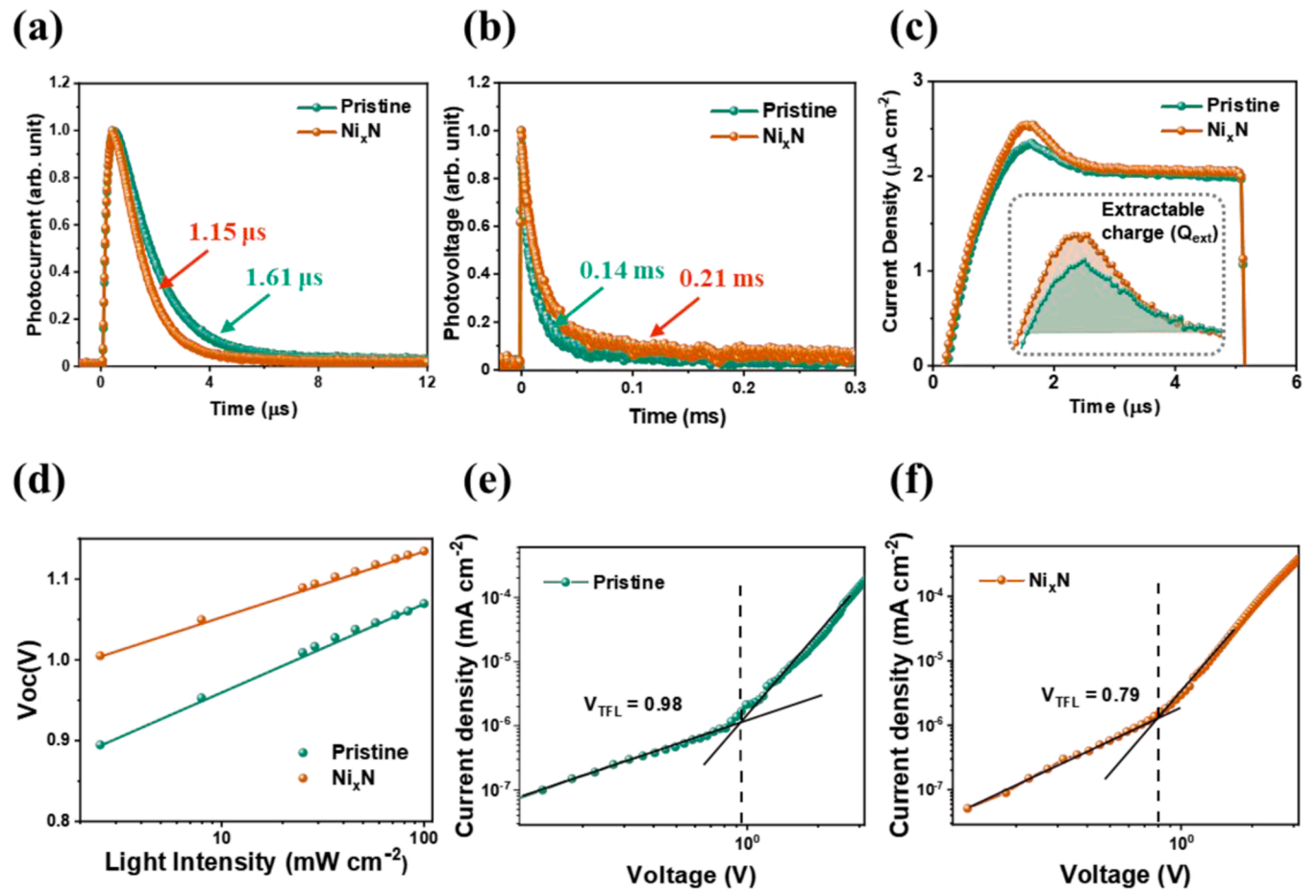

Fig. 4. (a) Transient photocurrent (TPC), (b) transient photovoltage (TPV), (c) photo-CELIV current transients (the inserted image is the current density at maximum peak (Δj)), and (d) light-intensity dependence on V_{OC} of pristine and Ni_xN-modified NiO_x-based devices. (e) Dark J-V characteristics of hole-only devices based on pristien and (f) Ni_xN-modified NiO_x thin films.

For a more detailed understanding of the improvement in charge carrier dynamics of Ni_xN-modified NiO_x-based devices, we performed a correlation analysis between interfacial defects and charge dynamics characteristics. First, to study the relationship between the charge recombination dynamics and defects in the device, V_{OC} dependence as a function of illuminating light intensity was measured under light intensities ranging from 2.5 to 100 mW cm^{-2}. As shown in the logarithmic scale curve of V_{OC} versus light intensity (Fig. 4d), the calculated ideality factor of the Ni_xN-modified NiO_x PSC was 1.35, significantly lower than that of NiO_x (1.82). If the device does no exhibit trap-assisted recombination, the ideality factor is generally 1, and if the value decreases close to this value, it is determined that the trap-assisted recombination has decreased. [62,63] From this point of view, it can be found that Ni_xN effectively suppressed the charge recombination, and the charge-trap site, which is the defect sites on the surface of the NiO_x, were decreased by Ni_xN. The change in trap density (N_t) was confirmed by the dark I-V curve of the hole-only device with planar structure comprising ITO substrate/HTL (NiO_x or Ni_xN-modified NiO_x)/perovskite/HTL (PTAA)/Ag (Fig. 4e-f). The trap density values in the two samples were determined to be 2.66×10^{15} cm^{-3} (NiO_x) and 1.11×10^{15} cm^{-3} (Ni_xN-modified NiO_x) when the corresponding trap filled limit voltage (V_{TFL}) values were 0.98 and 0.79 V, respectively. The low trap density of the Ni_xN-modified NiO_x supports the decrease the charge trap sites between NiO_x and perovskite and the passivation of defects on the surface of NiO_x by Ni_xN [48,49,64].

To verify that changes in the physical and electrical characteristics of NiO_x thin film by Ni_xN can be generalized and whether this approach can effectively reduce defects such as $Ni^{\geq 3+}$ species, we extended the series of XPS, UPS, photovoltaic characteristic, TPV, and TPC analyses to other NiO_x thin films, including overnight-treated NiO_x NPs thin film (OT-NiO_x NPs; 24-hour exposure in the atmosphere), NiO_x thin film prepared by sol-gel method (NiO_x SG), and overnight-treated SG (OT-NiO_x SG; 24-hour exposure in atmosphere). This expansion took into account situations that may occur in the general process, i.e., long-time atmospheric exposure of NiO_x thin film, and use of thin films prepared by other processes. Further, it was assumed that NiO_x thin films under long-term exposure to the atmosphere, or produced through other processes, would exhibit high concentrations of surface defects and other poor surface properties. Fig. S7 shows XPS spectra of the OT-NiO_x NPs, NiO_x SG, and OT-NiO_x SG thin films with and without NiN-treatment. Fig. 5a,b show the ratios of Ni_2O_3/NiO and NiOOH/NiO of nickel oxide species corresponding to the Ni $2p_{3/2}$ spectrum of each sample. When NiO_x NPs and NiO_x SG thin films were exposed to air for a long period, the ratio of Ni_2O_3/NiO decreased, while the ratio of NiOOH/NiO increased. Thus, it can be seen that defect sites and hydroxyl groups on the surface of the NiO_x thin film increase with overnight [2,34]. However, importantly, as NiN was deposited on the as-prepared and overnight NiO_x thin films, the Ni_2O_3/NiO ratio increased, while the NiOOH/NiO ratio decreased. Furthermore, these changes in chemical composition and relative ratio of nickel oxidation species for the Ni $2p_{3/2}$ of the NiO_x thin films (NiO_x NPs, OT-NiO_x NPs, NiO_x SG, and OT-NiO_x SG) were well consistent with changes in the O1s spectrum corresponding to NiN treatment (Fig. S7). Above all, as shown in Fig. S7, N 1 s signals indicating the formation of Ni_xN thin film, produced through chemical interaction between nickel nitrate and chemical species (defect sites and hydroxyl groups), were observed in all NiN-treated

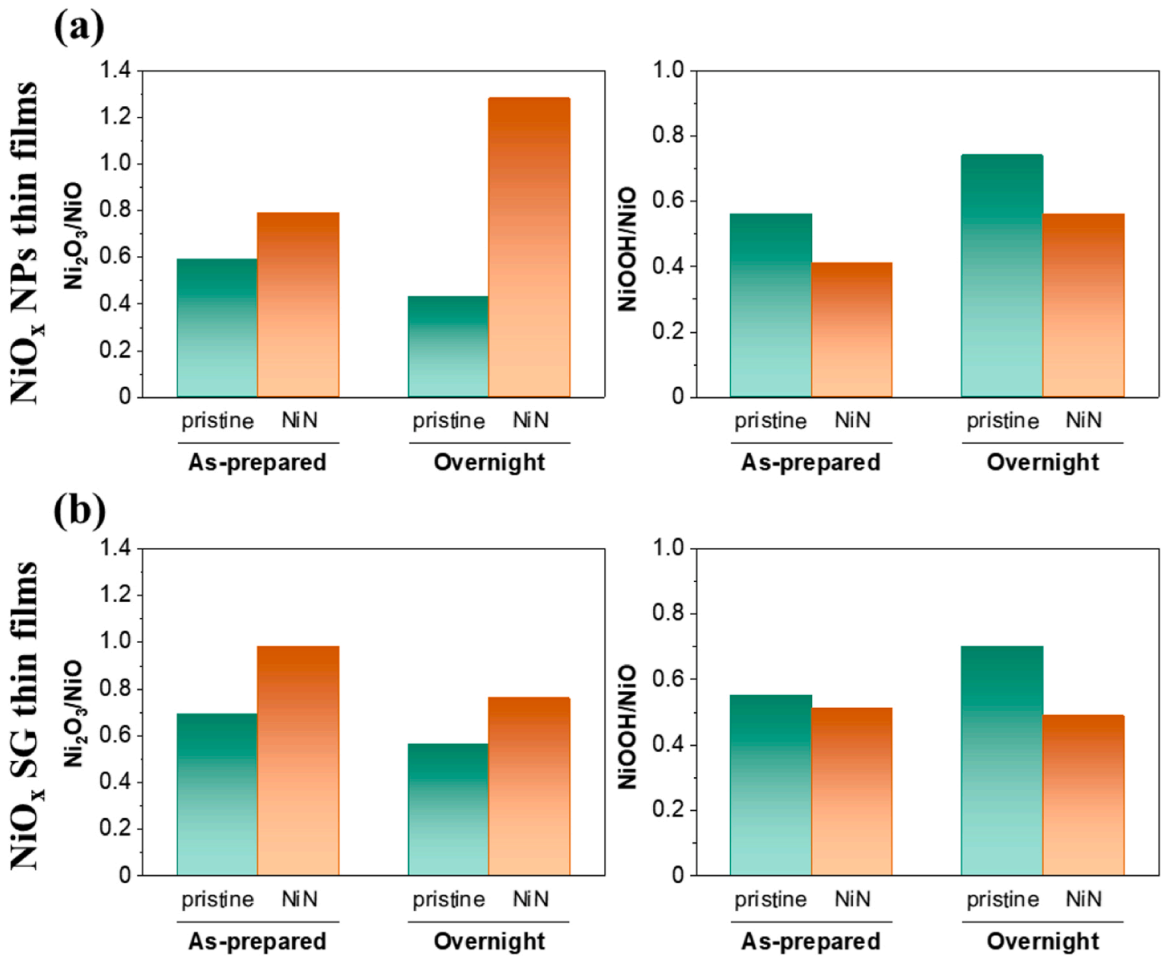

Fig. 5. Relative ratio of nickel oxidation species obtained from peak fitting of Ni $2p_{3/2}$ core level spectra of XPS of different type of NiO_x thin films.

samples. These results show that when NiN is applied to the surface of NiO_x thin film, the Ni_xN ultra-thin film is formed on the surface of the NiO_x thin film, Ni^{3+} chemical species on the surface of NiO_x thin film increase, while $Ni^{\geq 3+}$ chemical species decrease. As a result, it can be found that the surface treatment using NiN is an effective method to reduce defect sites and hydroxyl groups on the surface of NiO_x thin film.

The reduction of defect sites and hydroxyl groups on the NiO_x surface by use of NiN is also supported by work function changes and photoelectric properties. when NiN was deposited, that is, when Ni_xN was formed on as-prepared and overnight NiO_x thin films, cut-off edges shifted to higher levels of kinetic energy, resulting in higher value of WF than those of pristine NiO_x thin film (Fig. 6a-c). In addition, the corresponding calculated VBM was had a larger value than that of the pristine NiO_x thin film. These results indicate that energy level of Ni_xN-modified NiO_x is more suitable for high-performance PSCs, as shown in the band diagram in Fig. 2d. These results were demonstrated by the improved photovoltaic properties of Ni_xN-modified NiO_x-based PSCs. Fig. 6d-f illustrate the PCE histograms of the OT-NiO_x NPs, NiO_x SG, and OT-NiO_x SG thin films with and without Ni_xN-treatment, respectively. The OT-NiO_x NPs and OT-NiO_x SG based devices showed PCE values of 17.36% and 17.48%, respectively, lower than those of the pristine NiO_x SG and NiO_x NPs based devices (Table S2). Thus, this result demonstrates that high numbers of defect sites and hydroxyl groups weaken the performance of the PSC. In contrast, compared to those of pristine NiO_x-based devices, all Ni_xN-modified NiO_x-based devices showed more than 5% improvement in PCE. In particular, NiO_x NPs based devices showed PCE improvements of not less than 10% after Ni_xN treatment; surprisingly, the PCE of the OT-NiO_x NPs based device recovered to a value similar to that of the as-prepared NiO_x NPs based device. As described above (Fig. 4), this improvement in photovoltaic performance has been shown to be due to improvements in charge extraction and transportation capability by Ni_xN. All Ni_xN-modified NiO_x-devices had shorter TPC decay time than those of pristine NiO_x-devices, while TPV decay times were longer (Fig. 6g-i and Fig. S8), which indicates that better charge extraction and transportation were induced in devices by Ni_xN-modified NiO_x [12,49]. Through the extended experiments above, consequently, we confirmed that Ni_xN serves as a restorer to reduce defects such as $Ni^{\geq 3+}$ species on various NiO_x surfaces and ultimately to revivify the NiO_x-perovskite interface.

Finally, to verify the reliability of PSCs with Ni_xN-modified NiO_x, we performed stability testing while considering light, moisture and oxygen, and heat, all of which affect the long-term operational performance of the unencapsulated device. Fig. 7a shows the steady-state photocurrent density and PCE performance taken from the devices at maximum power point voltage under continuous illumination. We found that both pristine and Ni_xN-modified NiO_x-based devices have highly stabilized steady-state photocurrent outputs with considerable divergence (nearly 2.9%) from the initial efficiency. The Ni_xN-modified NiO_x-based devices achieved steady-state photocurrent density (20.30 mA cm^{-2}) and PCE (19.10%) in around 1800 s. However, the long-term operational stability of the devices under maximum power point tracking with continuous light irradiation showed significant divergence between unencapsulated pristine and Ni_xN-modified NiO_x-based devices (Fig. 7b). Ni_xN-modified NiO_x-based PSCs maintained about 69% of the original efficiency after 120 h, while pristine NiO_x-based PSCs totally degraded under the same conditions, indicating that the Ni_xN-modified

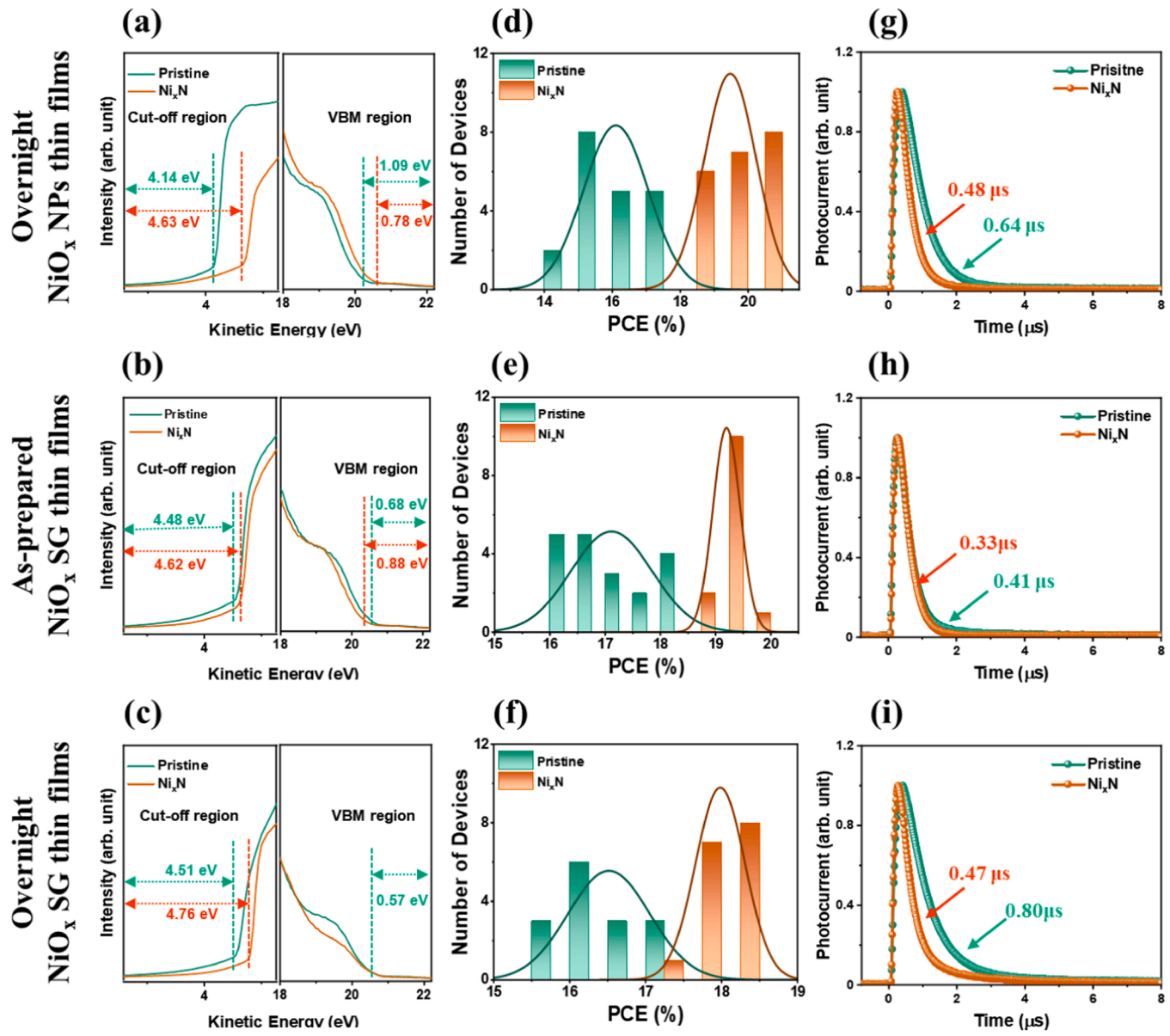

Fig. 6. Ultraviolet photoelectron spectroscopy spectra of pristine and NiN-treated NiO_x thin films: (a) overnight-treated NiO_x NPs, (b) as-prepared NiO_x SG, and (c) overnight-treated NiO_x SG thin films. Corresponding statistical histograms of PCEs and transient photocurrent (TPC) of pristine and NiN-treated NiO_x-based devices: (d, g) overnight-treated NiO_x NPs, (e, h) as-prepared NiO_x SG, and (f, i) overnight-treated NiO_x SG thin films.

NiO_x-based PSC have long-term light stability compared to the pristine NiO_x-based PSC. In addition, the operational stability under influences of moisture and oxygen was examined for unencapsulated PSCs for 1000 h under ambient conditions (25–30 ℃, 45–55% humidity), as shown in Fig. 7c. The Ni_xN-modified NiO_x-based device maintained about 82% of its initial efficiency after 1000 h, whereas that value for the pristine NiO_x-based device was 60%. These results show that the Ni_xN-modified NiO_x-based device has excellent resistance to moisture and oxygen compared to the pristine NiO_x-based device, thereby achieving long-term air stability. The thermal stability of unencapsulated pristine and Ni_xN-modified NiO_x-based devices was analyzed for more than 250 h using a hot-plate heated to 85℃ in a nitrogen-filled glove box (Fig. 7d). Pristine NiO_x-based devices almost entirely deteriorated after 200 h, but the Ni_xN-modified NiO_x-based device maintained more than 66% of its initial PCE in the harsh heat environment, while pristine NiO_x-based PSCs totally degraded, indicating that Ni_xN-modified NiO_x-based device has good thermal stability.

Importantly, these stability tests were performed on OT-NiO_x NPs, NiO_x SG, and OT-NiO_x SG based devices, and the results were consistent with the above results (Fig. S9). The operational performance of pristine OT-NiO_x NPs, NiO_x SG, and OT-NiO_x SG based devices decreased rapidly when they were exposed to long-term light, moisture and oxygen, and heat. In contrast, the operational performance of Ni_xN-modified OT-NiO_x NPs, NiO_x SG, and OT-NiO_x SG based devices decreased relatively gently. Therefore, it can be concluded that Ni_xN-modified NiO_x-based PSCs are more stable in operational conditions such as light, moisture and oxygen, and heat. It can be also inferred that, as shown in Fig. 7**e**, this improved stability was caused by the formation of a physicochemically stable Ni_xN interfacial thin film and thereby the prevention either defects ($Ni^{\geq 3+}$ sites) on the NiO_x surface or direct contact of perovskite with hydroxyl groups ($Ni^{\geq 3+}$ chemical species) on the NiO_x surface [38,65,66]. This is because that the hydroxyl group of on the NiO_x surface, i.e., the OH can easily react with $CH_3NH_3^+$ ion and PbI and form CH_3NH_2 and H_2O and PbO, respectively, causing perovskite decomposition [13,23]. Possible reaction mechanisms of the OH group with perovskite are the following

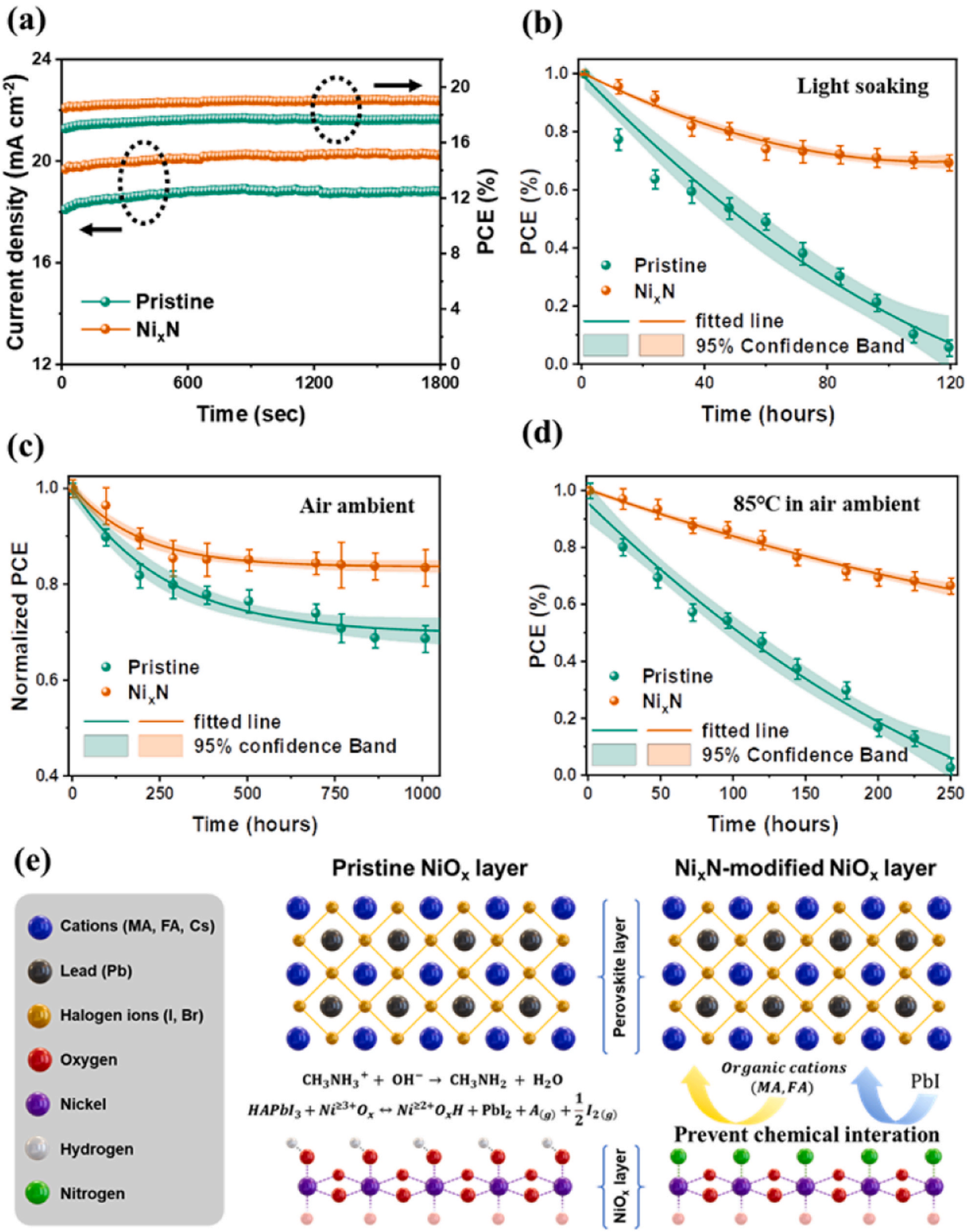

Fig. 7. (a) Steady-state photocurrent and PCE of pristine and Ni_xN-treated NiO_x-based devices measured at maximum power point under constant light illumination. (b) Light soaking stability of pristine and Ni_xN-treated NiO_x-based devices measured under constant light illumination. (c) Normalized PCE as function of time for pristine and Ni_xN-treated NiO_x-based devices in air ambient conditions. (d) Thermal stability under heating at 85 ℃ in air ambient condition. All devices were measured without encapsulation. (e) Schematic reaction of defect sites ($Ni^{\geq 3+}O_x$) and hydroxyl groups (OH) and perovskite that can occur on pristine and Ni_xN-modified NiO_x NPs thin films.

$$CH_3NH_3^+ + OH^- \rightarrow CH_3NH_2 + H_2O \quad (1)$$

$$PbI + OH \rightarrow PbO + HI \quad (2)$$

It has been also reported that $Ni^{\geq 3+}$ sites, due to their much higher oxidation potentials, can oxidize iodine chemical species [67]. Boyd et. al. revealed that $Ni^{\geq 3+}$ sites on the NiO_x surface act as Brønsted acid-bases, deprotonating from the A-site cations (CH_4N_2; FA and CH_3NH_2; MA) and oxidizing I^- [2]. They suggested that the reaction between the perovskite and NiO_x surfaces is as follows:

$$HAPbI_3 \leftrightarrow PbI_2 + HA^+ + I^- \quad (3)$$

$$HA^+ \leftrightarrow A_{(g)} + H^+ \quad (4)$$

$$I^- \leftrightarrow \frac{1}{2}I_{2(g)} + e^- \quad (5)$$

$$Ni^{\geq 3+}O_x + e^- + H^+ \leftrightarrow Ni^{\geq 2+}O_xH \quad (6)$$

$$HAPbI_3 + Ni^{\geq 3+}O_x \leftrightarrow Ni^{\geq 2+}O_xH + PbI_2 + A_{(g)} + \frac{1}{2}I_{2(g)} \quad (7)$$

where HA^+ is a protonated A-site cation ($CH_3NH_3^+$ or $CH_5N_2^+$) and A is the deprotonated A-site cation (CH_3NH_2 or CH_4N_2). This reaction indicates that the electrochemical reduction of $Ni^{\geq 3+}$ chemical species induces oxidation of iodine, and eventually volatile $\frac{1}{2}I_{2(g)}$ and $A_{(g)}$ can be formed. The consequent formation of $PbI_{2-x}Br_x$ can be derived from A-site cation depletion, which interferes with hole-extraction and transportation. The X-ray diffractogram of the pristine NiO_x NPs shows that $PbI_{2-x}Br_x$ phase (peak position 12.8°) was generated and the intensity of (001) peak (peak position 14.2°), an important characteristic of perovskite, was reduced (Fig. S10), which supports fast performance degradation due to lack of an A-site cation; the generation of the $PbI_{2-x}Br_x$ peak comes at the cost of degradation of the (001) peak of the perovskite layer and changes in the A-site cations in the perovskite layer can affect the arrangement of crystallographic planes [68,69]. On the other hand, no $PbI_{2-x}Br_x$ phase was observed in the XRD pattern of the NiO_x NPs thin film deposited Ni_xN, which satisfies requirements for maintaining more stable performance. This result has once again proved that Ni_xN acts as a restorer to reduce defects such as $Ni^{\geq 3+}$ species on various NiO_x surfaces and ultimately revives the NiO_x-perovskite interface by preventing a lack of A-site cations and the formation of $PbI_{2-x}Br_x$ phase. Furthermore, these results show that NiO_x surface treatment using NiN can be a promising and universal strategy to revive nickel oxide-perovskite interfaces and boost the performance and operational stability of perovskite solar cells.

Conclusion

In this study, for the first time, nickel nitrate was used as an interface modifier between NiO_x and perovskite layer to eliminate defect sites and hydroxyl groups on NiO_x surface. It was found that Ni_xN ultra-thin film can be formed on the NiO_x surface through spin coating of nickel nitrate solution at low temperatures; nickel nitrate reacted with defect sites and hydroxyl groups to form a uniform and ultra-thin Ni_xN layer on the NiO_x surface. XPS analysis proved that nitrogen atoms exist in various chemical states depending on the depth from the surface of the NiO_x NPs thin film. In addition, it was revealed that when Ni_xN applied on the surface of the NiO_x thin film, Ni^{3+} chemical species on the surface of the NiO_x thin film increased, while $Ni^{\geq 3+}$ chemical species decreased. Furthermore, Ni_xN led to better energy level alignment between the NiO_x HTL and the perovskite layer, resulting in improved charge extraction and transportation and reduced charge recombination. Consequently, the Ni_xN-modified NiO_x-based PSC recorded an outstanding efficiency of 20.45%, which is among the highest efficiency for inorganic interface modification layer-based PSCs reported to this date. Furthermore, this breakthrough approach has increased the operational stability of NiO_x-based PSCs. Ni_xN-modified NiO_x-based devices achieved steady-state photocurrent density of 20.30 mA cm^{-2} with 19.10% PCE and maintained about 69% of initial efficiency after 120 h continuous light irradiation. The unencapsulated Ni_xN-modified NiO_x-based PSC maintained about 82% of its initial efficiency after 1000 h; the Ni_xN-modified NiO_x-based PSC maintained more than 40% of its initial PCE in a harsh heat environment (85°C) for 200 h. These results demonstrate that this simple nickel nitrate treatment can be a promising and universal strategy to revive nickel oxide-perovskite interfaces by forming an Ni_xN interface modification layer, boosting the performance and operational stability of perovskite solar cells.

Experimental procedures

Experimental Procedures can be found in the Supplemental Information.

CRediT authorship contribution statement

Dilpreet Singh Mann: Conceptualization, Methodology, Formal analysis, Investigation, Writing – original draft. **Sung-Nam Kwon**: Conceptualization, Methodology, Formal analysis, Validation, Supervision, Visualization, Writing – review & editing. **Pramila Patil**: Formal analysis. **Seok-In Na**: Supervision, Writing – review & editing, Project administration, Funding acquisition.

Declaration of Competing Interest

The authors declare that they have no known competing financial interests or personal relationships that could have appeared to influence the work reported in this paper.

Data Availability

The data that has been used is confidential.

Acknowledgments

This research was supported by the Basic Science Research Program through the National Research Foundation of Korea (NRF) funded by the Ministry of Education (2020R1I1A1A01051961 and 2021R1A2C2010353).

Appendix A. Supporting information

Supplementary data associated with this article can be found in the online version at doi:10.1016/j.nanoen.2022.108062.

References

[1] NREL Best Research-Cell Efficiency Chart, ⟨https://www.nrel.gov/pv/cell-efficiency.html⟩ (accessed: February 2022).
[2] C.C. Boyd, R.C. Shallcross, T. Moot, R. Kerner, L. Bertoluzzi, A. Onno, S. Kavadiya, C. Chosy, E.J. Wolf, J. Werner, Overcoming redox reactions at perovskite-nickel oxide interfaces to boost voltages in perovskite solar cells, 4 (2020) pp. 1759–1775.
[3] Y. Bai, X. Meng, S. Yang, Interface engineering for highly efficient and stable planar p-i-n perovskite solar cells, 8 (2018) pp. 1701883.
[4] H. Chen, Q. Wei, M.I. Saidaminov, F. Wang, A. Johnston, Y. Hou, Z. Peng, K. Xu, W. Zhou, Z. Liu, Efficient and stable inverted perovskite solar cells incorporating secondary amines, 31 (2019) pp. 1903559.
[5] K.X. Steirer, R.E. Richards, A.K. Sigdel, A. Garcia, P.F. Ndione, S. Hammond, D. Baker, E.L. Ratcliff, C. Curtis, T. Furtak, D.S. Ginley, D.C. Olson, N.R. Armstrong, J. J. Berry, Nickel oxide interlayer films from nickel formate–ethylenediamine precursor: influence of annealing on thin film properties and photovoltaic device performance, 3 (2015) pp. 10949–10958.
[6] M. Jošt, T. Bertram, D. Koushik, J.A. Marquez, M.A. Verheijen, M.D. Heinemann, E. Köhnen, A. Al-Ashouri, S. Braunger, F. Lang, B. Rech, T. Unold, M. Creatore, I. Lauermann, C.A. Kaufmann, R. Schlatmann, S. Albrecht, 21.6%-Efficient Monolithic Perovskite/Cu(In,Ga)Se2 Tandem Solar Cells with Thin Conformal Hole

Transport Layers for Integration on Rough Bottom Cell Surfaces, 4 (2019) pp. 583–590.
[7] W.J. Scheideler, N. Rolston, O. Zhao, J. Zhang, R.H. Dauskardt, Rapid Aqueous Spray Fabrication of Robust NiOx: A Simple and Scalable Platform for Efficient Perovskite Solar Cells, 9 (2019) pp. 1803600.
[8] J. Xu, C.C. Boyd, Z.J. Yu, A.F. Palmstrom, D.J. Witter, B.W. Larson, R.M. France, J. Werner, S.P. Harvey, E.J. Wolf, W. Weigand, S. Manzoor, M.F.A.Mv Hest, J.J. Berry, J.M. Luther, Z.C. Holman, M.D. McGehee, Triple-halide wide–band gap perovskites with suppressed phase segregation for efficient tandems, 367 (2020) pp. 1097–1104.
[9] E. Aydin, J. Troughton, M. De Bastiani, E. Ugur, M. Sajjad, A. Alzahrani, M. Neophytou, U. Schwingenschlögl, F. Laquai, D. Baran, S. De Wolf, Room-Temperature-Sputtered Nanocrystalline Nickel Oxide as Hole Transport Layer for p–i–n Perovskite Solar Cells, 1 (2018) pp. 6227–6233.
[10] M. Stolterfoht, C.M. Wolff, J.A. Márquez, S. Zhang, C.J. Hages, D. Rothhardt, S. Albrecht, P.L. Burn, P. Meredith, T. Unold, D. Neher, Visualization and suppression of interfacial recombination for high-efficiency large-area pin perovskite solar cells, Nat. Energy 3 (2018) 847–854.
[11] Y. Hou, W. Chen, D. Baran, T. Stubhan, N.A. Luechinger, B. Hartmeier, M. Richter, J. Min, S. Chen, C.O. Quiroz, N. Li, H. Zhang, T. Heumueller, G.J. Matt, A. Osvet, K. Forberich, Z.G. Zhang, Y. Li, B. Winter, P. Schweizer, E. Spiecker, C.J. Brabec, Overcoming the interface losses in planar heterojunction perovskite-based solar cells, Adv. Mater. 28 (2016) 5112–5120.
[12] P. Patil, D.S. Mann, U.T. Nakate, Y.-B. Hahn, S.-N. Kwon, S.-I. Na, Hybrid interfacial ETL engineering using PCBM-SnS2 for High-Performance p-i-n structured planar perovskite solar cells, 397 (2020) pp. 125504.
[13] D.S. Mann, P. Patil, S.-N. Kwon, S.-I. Na, Enhanced performance of pin perovskite solar cell via defect passivation of nickel oxide/perovskite interface with self-assembled monolayer, 560 (2021) pp. 149973.
[14] X. Yin, Y. Guo, H. Xie, W. Que, L.B. Kong, Nickel oxide as efficient hole transport materials for perovskite solar cells, Sol. RRL 3 (2019) 1900001.
[15] Y. Guo, X. Yin, J. Liu, Y. Yang, W. Chen, M. Que, W. Que, B. Gao, Annealing atmosphere effect on Ni states in the thermal-decomposed NiOx films for perovskite solar cell application, Electrochim. Acta 282 (2018) 81–88.
[16] W. Chen, Y. Zhou, L. Wang, Y. Wu, B. Tu, B. Yu, F. Liu, H.-W. Tam, G. Wang, A. B. Djurišić, L. Huang, Z. He, Molecule-doped nickel oxide: verified charge transfer and planar inverted mixed cation perovskite solar cell, Adv. Mater. 30 (2018) 1800515.
[17] Q. Wang, C.-C. Chueh, T. Zhao, J. Cheng, M. Eslamian, W.C.H. Choy, A.K.-Y. Jen, Effects of self-assembled monolayer modification of nickel oxide nanoparticles layer on the performance and application of inverted perovskite solar cells, ChemSusChem 10 (2017) 3794–3803.
[18] D. Ouyang, Z. Huang, W.C.H. Choy, Solution-processed metal oxide nanocrystals as carrier transport layers in organic and perovskite solar cells, Adv. Funct. Mater. 29 (2019) 1804660.
[19] J.H. Kim, P.W. Liang, S.T. Williams, N. Cho, C.C. Chueh, M.S. Glaz, D.S. Ginger, A. K.Y. Jen, High-performance and environmentally stable planar heterojunction perovskite solar cells based on a solution-processed copper-doped nickel oxide hole-transporting layer, 27 (2015) pp. 695–701.
[20] W. Chen, Y. Wu, Y. Yue, J. Liu, W. Zhang, X. Yang, H. Chen, E. Bi, I. Ashraful, M. Grätzel, Efficient and stable large-area perovskite solar cells with inorganic charge extraction layers, 350 (2015) pp. 944–948.
[21] W. Chen, F.Z. Liu, X.Y. Feng, A.B. Djurišić, W.K. Chan, Z.B. He, Cesium doped NiOx as an efficient hole extraction layer for inverted planar perovskite solar cells, 7 (2017) pp. 1700722.
[22] K. Yao, F. Li, Q. He, X. Wang, Y. Jiang, H. Huang, A.K.-Y. Jen, A copper-doped nickel oxide bilayer for enhancing efficiency and stability of hysteresis-free inverted mesoporous perovskite solar cells, 40 (2017) pp. 155–162.
[23] D.S. Mann, P. Patil, D.-H. Kim, S.-N. Kwon, S.-I. Na, Boron nitride-incorporated NiOx as a hole transport material for high-performance pin planar perovskite solar cells, 477 (2020) pp. 228738.
[24] C. Hu, Y. Bai, S. Xiao, K. Tao, W.K. Ng, K.S. Wong, S.H. Cheung, S.K. So, Q. Chen, S. Yang, Surface Sulfuration of NiO Boosts the Performance of Inverted Perovskite Solar Cells, 4 (2020) pp. 2000270.
[25] Q. Wang, C.C. Chueh, T. Zhao, J. Cheng, M. Eslamian, W.C.H. Choy, A.K. Jen, Effects of Self-Assembled Monolayer Modification of Nickel Oxide Nanoparticles Layer on the Performance and Application of Inverted Perovskite Solar Cells, 10 (2017) pp. 3794–3803.
[26] N. Singh, Y.T. Tao, Effect of surface modification of nickel oxide hole-transport layer via self-assembled monolayers in perovskite solar cells, 2 (2021) pp. 2390–2399.
[27] H. Cheng, Y. Li, G. Zhao, K. Zhao, Z.-S. Wang, Pyridine-Terminated Conjugated Organic Molecules as an Interfacial Hole Transfer Bridge for NiOx-Based Perovskite Solar Cells, 11 (2019) pp. 28960–28967.
[28] R. Wang, M. Mujahid, Y. Duan, Z.K. Wang, J. Xue, Y. Yang, A Review of Perovskites Solar Cell Stability, 29 (2019) pp. 1808843.
[29] M.-S. Balogun, Y. Zeng, W. Qiu, Y. Luo, A. Onasanya, T.K. Olaniyi, Y. Tong, Three-dimensional nickel nitride (Ni3N) nanosheets: free standing and flexible electrodes for lithium ion batteries and supercapacitors, 4 (2016) pp. 9844–9849.
[30] M. Shalom, D. Ressnig, X. Yang, G. Clavel, T.P. Fellinger, M. Antonietti, Nickel nitride as an efficient electrocatalyst for water splitting, 3 (2015) pp. 8171–8177.
[31] J. Soo Kang, M.-A. Park, J.-Y. Kim, S. Ha Park, D. Young Chung, S.-H. Yu, J. Kim, J. Park, J.-W. Choi, K. Jae Lee, J. Jeong, M. Jae Ko, K.-S. Ahn, Y.-E. Sung, Reactively sputtered nickel nitride as electrocatalytic counter electrode for dye- and quantum dot-sensitized solar cells, 5 (2015) pp. 10450.
[32] F. Wang, X. Li, J. Du, H. Duan, H. Wang, Y. Gou, L. Yang, L. Fan, J. Yang, F. Rosei, Coordinating light management and advance metal nitride interlayer enables MAPbI3 solar cells with >21.8% efficiency, 92 (2022) pp. 106765.
[33] Y.-J. Shih, Y.-H. Huang, C.P. Huang, Electrocatalytic ammonia oxidation over a nickel foam electrode: Role of Ni(OH)2(s)-NiOOH(s) nanocatalysts, 263 (2018) pp. 261–271.
[34] Z. Wang, Z. Luo, C. Zhao, Q. Guo, Y. Wang, F. Wang, X. Bian, A. Alsaedi, T. Hayat, Za Tan, Efficient and Stable Pure Green All-Inorganic Perovskite CsPbBr3 Light-Emitting Diodes with a Solution-Processed NiOx Interlayer, 121 (2017) pp. 28132–28138.
[35] E.L. Ratcliff, J. Meyer, K.X. Steirer, A. Garcia, J.J. Berry, D.S. Ginley, D.C. Olson, A. Kahn, N.R. Armstrong, Evidence for near-Surface NiOOH Species in Solution-Processed NiOx Selective Interlayer Materials: Impact on Energetics and the Performance of Polymer Bulk Heterojunction Photovoltaics, 23 (2011) pp. 4988–5000.
[36] N. Pant, A. Kulkarni, M. Yanagida, Y. Shirai, T. Miyasaka, K. Miyano, Investigating the Growth of CH3NH3PbI3 Thin Films on RF-Sputtered NiOx for Inverted Planar Perovskite Solar Cells: Effect of CH3NH3+ Halide Additives versus CH3NH3+ Halide Vapor Annealing, 7 (2020) pp. 1901748.
[37] Z. Wang, L. Xu, F. Huang, L. Qu, J. Li, K.A. Owusu, Z. Liu, Z. Lin, B. Xiang, X. Liu, Copper–nickel nitride nanosheets as efficient bifunctional catalysts for hydrazine-assisted electrolytic hydrogen production, 9 (2019) pp. 1900390.
[38] J.S. Kang, M.-A. Park, J.-Y. Kim, S.H. Park, D.Y. Chung, S.-H. Yu, J. Kim, J. Park, J.-W. Choi, K.J. Lee, Reactively sputtered nickel nitride as electrocatalytic counter electrode for dye-and quantum dot-sensitized solar cells, 5 (2015) pp. 1–11.
[39] J. Baltrusaitis, P.M. Jayaweera, V.H. Grassian, XPS study of nitrogen dioxide adsorption on metal oxide particle surfaces under different environmental conditions, 11 (2009) pp. 8295–8305.
[40] P. Zhou, B. Li, Z. Fang, W. Zhou, M. Zhang, W. Hu, T. Chen, Z. Xiao, S. Yang, Nitrogen-Doped Nickel Oxide as Hole Transport Layer for High-Efficiency Inverted Planar Perovskite Solar Cells, 3 (2019) pp. 1900164.
[41] P.S. Chandrasekhar, Y.-H. Seo, Y.-J. Noh, S.-I. Na, Room temperature solution-processed Fe doped NiOx as a novel hole transport layer for high efficient perovskite solar cells, 481 (2019) pp. 588–596.
[42] S. Park, M.-S. Kim, W. Jang, J.K. Park, D.H. Wang, Covalent organic nanosheets for effective charge transport layers in planar-type perovskite solar cells, 10 (2018) pp. 4708–4717.
[43] Z. He, C. Zhong, X. Huang, W.Y. Wong, H. Wu, L. Chen, S. Su, Y. Cao, Simultaneous enhancement of open-circuit voltage, short-circuit current density, and fill factor in polymer solar cells, 23 (2011) pp. 4636–4643.
[44] J.-S. Yeo, M. Kang, Y.-S. Jung, R. Kang, S.-H. Lee, Y.-J. Heo, S.-H. Jin, D.-Y. Kim, S.-I. Na, In-depth considerations for better polyelectrolytes as interfacial materials in polymer solar cells, 21 (2016) pp. 26–38.
[45] X. Dai, Z. Zhang, Y. Jin, Y. Niu, H. Cao, X. Liang, L. Chen, J. Wang, X. Peng, Solution-processed, high-performance light-emitting diodes based on quantum dots, 515 (2014) pp. 96–99.
[46] Q. Wang, Q. Dong, T. Li, A. Gruverman, J. Huang, Thin insulating tunneling contacts for efficient and water-resistant perovskite solar cells, 28 (2016) pp. 6734–6739.
[47] J.-H. Yu, C.-H. Lee, H.-I. Joh, J.-S. Yeo, S.-I. Na, Synergetic effects of solution-processable fluorinated graphene and PEDOT as a hole-transporting layer for highly efficient and stable normal-structure perovskite solar cells, 9 (2017) pp. 17167–17173.
[48] M.-J. Choi, Y.-S. Lee, I.H. Cho, S.S. Kim, D.-H. Kim, S.-N. Kwon, S.-I. Na, Functional additives for high-performance inverted planar perovskite solar cells with exceeding 20% efficiency: Selective complexation of organic cations in precursors, 71 (2020) pp. 104639.
[49] Y.-J. Kang, S.-N. Kwon, S.-P. Cho, Y.-H. Seo, M.-J. Choi, S.-S. Kim, S.-I. Na, Antisolvent additive engineering containing dual-function additive for triple-cation p–i–n perovskite solar cells with over 20% PCE, 5 (2020) pp. 2535–2545.
[50] C.R. McNeill, I. Hwang, N.C. Greenham, Photocurrent transients in all-polymer solar cells: Trapping and detrapping effects, 106 (2009) pp. 024507.
[51] D. Kiermasch, P. Rieder, K. Tvingstedt, A. Baumann, V. Dyakonov, Improved charge carrier lifetime in planar perovskite solar cells by bromine doping, 6 (2016) pp. 39333.
[52] Y. Guo, H. Lei, L. Xiong, B. Li, G. Fang, An integrated organic–inorganic hole transport layer for efficient and stable perovskite solar cells, 6 (2018) pp. 2157–2165.
[53] S.-N. Kwon, J.-H. Yu, S.-I. Na, A systematic approach to ZnO nanoparticle-assisted electron transport bilayer for high efficiency and stable perovskite solar cells, 801 (2019) pp. 277–284.
[54] Z. Liu, A. Zhu, F. Cai, L. Tao, Y. Zhou, Z. Zhao, Q. Chen, Y.-B. Cheng, H. Zhou, Nickel oxide nanoparticles for efficient hole transport in pin and nip perovskite solar cells, 5 (2017) pp. 6597–6605.
[55] S. Xiao, C. Hu, H. Lin, X. Meng, Y. Bai, T. Zhang, Y. Yang, Y. Qu, K. Yan, J. Xu, Integration of inverse nanocone array based bismuth vanadate photoanodes and bandgap-tunable perovskite solar cells for efficient self-powered solar water splitting, 5 (2017) pp. 19091–19097.
[56] D.S. Mann, Y.-H. Seo, S.-N. Kwon, S.-I. Na, Efficient and stable planar perovskite solar cells with a PEDOT: PSS/SrGO hole interfacial layer, 812 (2020) pp. 152091.
[57] N. Ahn, D.-Y. Son, I.-H. Jang, S.M. Kang, M. Choi, N.-G. Park, Highly Reproducible Perovskite Solar Cells with Average Efficiency of 18.3% and Best Efficiency of 19.7% Fabricated via Lewis Base Adduct of Lead(II) Iodide, 137 (2015) pp. 8696–8699.
[58] Y. Chen, J. Peng, D. Su, X. Chen, Z. Liang, Efficient and balanced charge transport revealed in planar perovskite solar cells, 7 (2015) pp. 4471–4475.

[59] M. Stephen, K. Genevičius, G. Juška, K. Arlauskas, R.C. Hiorns, Charge transport and its characterization using photo-CELIV in bulk heterojunction solar cells, 66 (2017) pp. 13–25.
[60] M. Neukom, S. Zufle, S. Jenatsch, B. Ruhstaller, Opto-electronic characterization of third-generation solar cells, 19 (2018) pp. 291–316.
[61] J. Peng, Y. Chen, K. Zheng, T. Pullerits, Z. Liang, Insights into charge carrier dynamics in organo-metal halide perovskites: from neat films to solar cells, 46 (2017) pp. 5714–5729.
[62] C.M. Proctor, M. Kuik, T.-Q. Nguyen, Charge carrier recombination in organic solar cells, 38 (2013) pp. 1941–1960.
[63] G.J.A. Wetzelaer, M. Scheepers, A.M. Sempere, C. Momblona, J. Ávila, H.J. Bolink, Trap-assisted non-radiative recombination in organic–inorganic perovskite solar cells, 27 (2015) pp. 1837–1841.
[64] F. Zhang, S. Ye, H. Zhang, F. Zhou, Y. Hao, H. Cai, J. Song, J. Qu, Comprehensive passivation strategy for achieving inverted perovskite solar cells with efficiency exceeding 23% by trap passivation and ion constraint, (2021) pp. 106370.
[65] X. Zheng, B. Chen, J. Dai, Y. Fang, Y. Bai, Y. Lin, H. Wei, Xiao C. Zeng, J. Huang, Defect passivation in hybrid perovskite solar cells using quaternary ammonium halide anions and cations, 2 (2017) pp. 17102.
[66] W. Chen, Y. Zhou, L. Wang, Y. Wu, B. Tu, B. Yu, F. Liu, H.W. Tam, G. Wang, A.B. Djurišić, Molecule-doped nickel oxide: verified charge transfer and planar inverted mixed cation perovskite solar cell, 30 (2018) pp. 1800515.
[67] M. Antelman, The Encyclopedia of Chemical Electrode Potentials, Springer Science & Business Media, 2012.
[68] I. Kamal, Y. Bas, Materials Today: Proceedings, (2021).
[69] G. Zheng, C. Zhu, J. Ma, X. Zhang, G. Tang, R. Li, Y. Chen, L. Li, J. Hu, J. Hong, Manipulation of facet orientation in hybrid perovskite polycrystalline films by cation cascade, 9 (2018) pp. 1–11.